Received: 25 February 2021 | Revised: 25 May 2021 | Accepted: 3 June 2021

DOI: 10.1002/bit.27866

ARTICLE

BIOTECHNOLOGY AND BIOENGINEERING WILEY

Engineered modular microphysiological models of the human airway clearance phenomena

Lucia Pedersoli[1] | Shuaizhong Zhang[2,3] | Francesco Briatico-Vangosa[1] | Paola Petrini[1] | Ruth Cardinaels[2,4] | Jaap den Toonder[2,3] | Daniela Peneda Pacheco[1]

[1]Department of Chemistry, Materials and Chemical Engineering "Giulio Natta", Politecnico di Milano, Milan, Italy

[2]Department of Mechanical Engineering, Eindhoven University of Technology, Eindhoven, The Netherlands

[3]Institute for Complex Molecular Systems, Eindhoven University of Technology, Eindhoven, The Netherlands

[4]Soft Matter Rheology and Technology, Department of Chemical Engineering, KU Leuven, Heverlee, Belgium

Correspondence

Dr. Daniela Peneda Pacheco, Department of Chemistry, Materials and Chemical Engineering "Giulio Natta," Politecnico di Milano, Piazza Leonardo da Vinci, 32, 20133 Milan, Italy.
Email: danielapatricia.peneda@polimi.it

Present address

Shuaizhong Zhang, Physical Intelligence Department, Max Planck Institute for Intelligent Systems, Stuttgart, Germany.

Funding information

Switch2Product, Grant/Award Number: UA.A.RRR.ARICID.SVRA.AUTO.AZ18VARI10; European Research Council (ERC): Bio-Inspired Microfluidics Platform for Biomechanical Analysis, Grant/Award Number: 833214

Abstract

Mucociliary clearance is a crucial mechanism that supports the elimination of inhaled particles, bacteria, pollution, and hazardous agents from the human airways, and it also limits the diffusion of aerosolized drugs into the airway epithelium. In spite of its relevance, few in vitro models sufficiently address the cumulative effect of the steric and interactive barrier function of mucus on the one hand, and the dynamic mucus transport imposed by ciliary mucus propulsion on the other hand. Here, ad hoc mucus models of physiological and pathological mucus are combined with magnetic artificial cilia to model mucociliary transport in both physiological and pathological states. The modular concept adopted in this study enables the development of mucociliary clearance models with high versatility since these can be easily modified to reproduce phenomena characteristic of healthy and diseased human airways while allowing to determine the effect of each parameter and/or structure separately on the overall mucociliary transport. These modular airway models can be available off-the-shelf because they are exclusively made of readily available materials, thus ensuring reproducibility across different laboratories.

KEYWORDS

cilia, dynamic systems, microphysiological models, mucociliary clearance, mucus

1 | INTRODUCTION

Mucus is a three-dimensional hydrogel laying over the human airway epithelium that constitutes its primary innate self-defense barrier. Along the respiratory tract, mucus is supported by the periciliary layer (PCL), a watery intermediate blanket between the mucus and the underlying airway epithelium. PCL consists of a low viscous liquid within which tethered mucins are present in an undefined quantity (Button et al., 2012). Inside this layer, cilia (hair-*like* motile structures) located on the luminal surface of ciliated cells are responsible for mucus propulsion and transport along with the respiratory system. Cilia can move asymmetrically in space and time at a frequency of 10–15 Hz, with consecutive cilia moving slightly out-of-phase (Droguett et al., 2017; Khelloufi et al., 2018; Murgia et al., 2018). Thanks to this, cilia are able to generate a wave that travels over the envelop of their tips, and by this so-called metachronal motion, mucus and mucus-entrapped inhaled particles are constantly transported towards the oropharyngeal region to be expectorated or swallowed (Fahy & Dickey, 2010; Livraghi & Randell, 2007; Sears et al., 2015).

The result of the harmonized interaction between mucus, PCL, and cilia constitutes the mucociliary clearance (MCC) apparatus. In physiological conditions, this innate self-defense mechanism guarantees that inhaled particles, bacteria, pollution, and hazardous agents entrapped within mucus are further eliminated due to cilia propulsion (Henning et al., 2008; Livraghi & Randell, 2007). Unfortunately, this mechanism is hampered in airway disorders, like cystic fibrosis (CF), chronic obstructive pulmonary disease (COPD), asthma, or primary dyskinesia (Livraghi & Randell, 2007; Sears et al., 2015). CF is a life-threatening genetic disease associated with a mutation at the CF transmembrane conductance regulator channel. In physiological conditions, this channel coordinates the passage of chloride, sodium, and bicarbonate ions across the airway epithelium (Livraghi & Randell, 2007). In pathological conditions, however, dysfunctions at these channels cause reduced chloride and bicarbonate secretions and increased sodium absorption. As a result, thickened and sticky mucus secretions, exhibiting altered chemical composition, structure and viscoelastic properties, are characteristic of CF patients. Along with abnormal mucus, the unbalanced ion exchange also leads to PCL depletion that limits ciliary beating. Reduced or hampered mucociliary transport, in turn, generates mucus accumulation and stagnation to the point where opportunistic bacteria may colonize the airways and form large colonies and biofilms, protecting these bacteria from the action of both immune system and pharmacological treatment (Bhagirath et al., 2016; Livraghi & Randell, 2007; Worlitzsch et al., 2002).

Modeling airway cilia hydrodynamics and its correlated mucus transport is really challenging since it involves not only ciliary motion under the influence of driving forces (i.e., ciliary dynamics associated with mucus propulsion) but also the coupling effect between cilia and the overlying fluids and the resulting mucus propulsion (Norton et al., 2011). As a consequence, the overall resulting problem is nonlinear and very difficult to replicate in a laboratory setting. In addition, there is a large variability of viscoelastic properties from subject-to-subject and depending on the type of airway disorder, which further increases the complexity of such physio(patho)logical phenomenon. Thus, most available models of physiological MCC are numerical models based on hypotheses aimed at simplifying the complex non-Newtonian viscoelastic behavior of mucus, with or without the presence of the PCL (Norton et al., 2011; Sedaghat et al., 2016). Other studies exploiting in vitro cell monolayers or ex vivo models are instead expensive, time-consuming, exhibit high interlaboratory variability, and do not separately consider the effects of PCL versus mucus and its transport (Henning et al., 2008; Khelloufi et al., 2018; Lorenzi et al., 1992; Sears et al., 2015). An example is the small airway-on-a-chip engineered to study lung inflammation and drug responses in vitro, which relies on a microfluidic device made of polydimethylsiloxane (PDMS) containing mucociliary bronchiolar epithelium and an underlying microvascular endothelium cultured at an air–liquid interface (Benam et al., 2016). This system exhibits various physiological parameters. Yet, neither the existence of the PCL nor the amount of mucus was reported. Additionally, it requires 3–5 weeks of cell culture to ensure ciliary beating (Benam et al., 2016). In CF conditions, the large variability in viscoelastic properties that occurs not only between patients but also within a single patient during the day requires personalized mucus models to match the properties of the mucus collected from the patient. Few models have addressed the MCC apparatus in pathological states exploiting cellular monolayers (Birket et al., 2014). Indeed, most of the studies that involve CF mucus are focused on drug diffusion without considering that also PCL depletion and cilia compression under the overlying mucus have an important impact on pharmacological treatment, disease progression, and lung degeneration (Hill et al., 2018; Liu et al., 2014).

In vitro models that reproduce the complexity of the airway MCC may enable a closer determination of the time of drug retention and elimination so that concentrations can be adjusted to guarantee pharmacological efficiency to overcome drug elimination due to mucus transport. Microphysiological models may also provide a better understanding of mucociliary transport in both physiological and pathological scenarios when these are reproducible and customizable. With this in mind, we propose an innovative concept to engineer modular microphysiological models of human airway MCC in both physiological and CF states by coupling ad hoc models of physiological and pathological mucus with magnetic artificial cilia (MAC) to model MCC. To do so, the MCC apparatus was decomposed into three different units: mucus, PCL, and cilia (Figure 1a,b). This modular concept enabled the design of modular models of the MCC apparatus (Figure 1c), as each unit may be individually modified to closely model the characteristics of the MCC apparatus of different patients, according to age, type of disease, smoking habits, among others. Both L-Mu^{3}Gel and CF-Mu^{3}Gel are available mucus models and these were adopted as models of physiological and CF mucus, respectively. L-Mu^{3}Gel and CF-Mu^{3}Gel exhibit chemical composition, viscoelastic properties, and structure similar to that of native human mucus. The ability to tune the viscoelastic properties of the mucus models opens the possibility to study MCC in a patient-specific manner. Optimized MACs were exploited to model airway cilia by modifying a cleanroom protocol previously proposed by Zhang et al. (2018). These MACs exhibit tailorable movement and beating frequency, moving asymmetrically in space and time. The fabricated MACs beat asymmetrically in space and time and are able to generate metachronal waves mimicking physiological airway cilia, by imposing a phase lag between consecutive cilia through external actuation using a magnet belt (Zhang et al., 2020). Up to our knowledge, it is the first time that artificial cilia are exploited to produce microphysiological models of the human airway MCC. To model physiological mucociliary transport, an intermediate PCL-simulant was introduced to support the transport of L-Mu^{3}Gel by the MAC, as observed in the physiological human airway. Both water and glycerol were chosen as PCL simulants, due to their different viscosities expected to impact ciliary motion. When water is employed as a PCL simulant, L-Mu^{3}Gel moves at a speed ten times higher than with a glycerol PCL-simulant. When CF-Mu^{3}Gel was

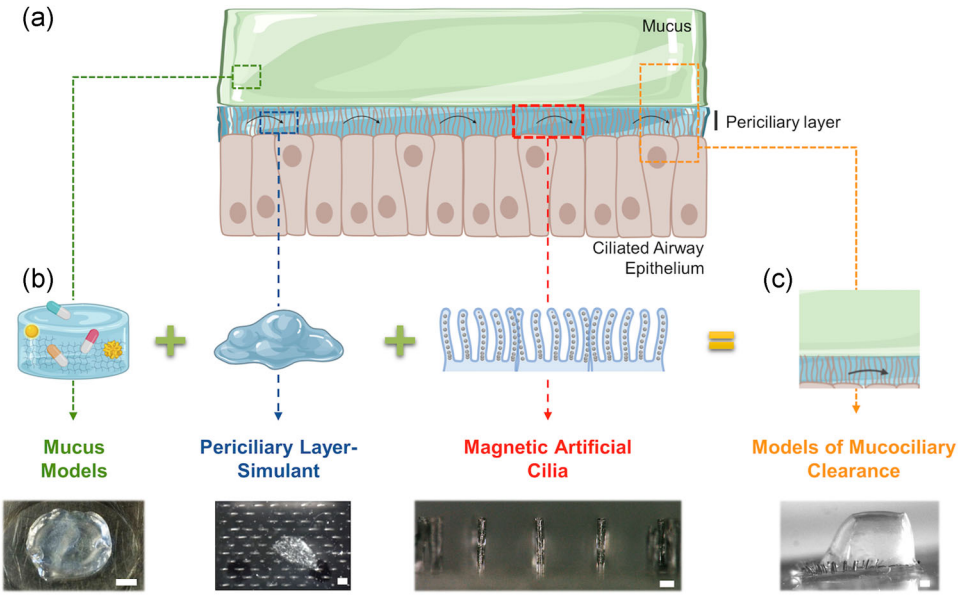

FIGURE 1 Schematic representation of the modular concept employed in this study, which takes inspiration from the human mucociliary clearance (MCC) apparatus. Both physiological and pathological models of the MCC apparatus were produced by identifying and combining, in a modular fashion, structures and parameters impacting mucociliary transport. (a) Schematic representation of human airway apparatus. (b) Mucus, periciliary layer, and cilia were selected as units affecting mucociliary transport. Their physicochemical properties were changed to produce different mucus models and to test different PCL-simulants and ciliated structures. (c) These units were finally coupled to engineer models of the physiological and CF MCC apparatus. The scale bars correspond to 100 μm. CF, cystic fibrosis; PCL, periciliary layer.

coupled to the MAC, it was observed that cilia were compressed and showed absent or negligible motion, a phenomenon resembling that observed in CF patients. Herein, we provide a versatile and innovative concept that can be further adapted to produce *in-scale* models of airway MCC and to closely model biological phenomena of airway-associated disorders.

2 | MATERIALS AND METHODS

2.1 | Materials

MAC was fabricated exploiting a mold created on a silicon wafer using SU-8 2150 negative photoresist (Permanent Epoxy Negative Photoresist; Microchem). The MAC was made of a magnetic precursor mixture consisting of thermally curable PDMS (Sylgard184; Dow Corning) and magnetic carbonyl iron powder (99.5%, 5 μm particle size), as previously described (Zhang et al., 2018; see Supporting Information 1—fabrication of the MAC for more details). Degradation studies were carried out using ethylenediaminetetraacetic acid (EDTA; E9884) and sodium hydroxide (NaOH; S5881). All products were supplied by Sigma-Aldrich. L-Mu^{3}Gel and CF-Mu^{3}Gel were adopted as models of physiological and pathological airway mucus, respectively. These were purposely produced with the proprietary expertize of Bac^{3}Gel, Lda, Portugal ("Www.Bac3Gel.Com"). Both L-Mu^{3}Gel and CF-Mu^{3}Gel are composed of commercial mucin from porcine stomach type III (M1778; Lot # SLBQ7188V; Sigma-Aldrich), which contains Muc5AC, one of the most important mucins found in airway mucus (Harding, 1989). Commercially available mucins are easily available and offer higher consistency among different laboratories than those isolated by different research groups. L-Mu^{3}Gel was introduced over the MAC to reproduce physiological MCC, while CF-Mu^{3}Gel was introduced over the MAC to model the pathological CF MCC. Before coupling these mucus models with MAC, these were submitted to rheological characterization and to define their consistency. CF-Mu^{3}Gels with different viscoelastic properties were tested to model the variations of CF mucus properties occurring within a single day or during different days and/or among different patients.

2.2 | Rheological characterization

The viscoelastic properties of both L-Mu^{3}Gel and CF-Mu^{3}Gel exhibiting different crosslinking degrees were determined by rheological characterization (Anton Paar Rheometer MCR502) using a 50-mm diameter plate geometry at 25°C. The investigation was carried out through oscillatory testing. The linear viscoelastic region (LVR) of the different mucus models was determined through strain sweep analyses by employing a strain sweep varying from 0.1% to 1000% at a frequency of 1 Hz. Frequency sweeps were further performed to evaluate both storage, G', and loss, G'', moduli, as well as the complex shear

modulus, G^*, at a strain amplitude of 0.5% (within the LVR) with a frequency sweep ranging from 0.1 to 20 Hz (to include breathing frequency, 0.5 Hz, and ciliary beating frequency, 10 Hz, under physiologic conditions). The duration of the experiments was approximately 10 min, which was sufficiently short to exclude drying of the mucus models during characterization.

2.3 | Fabrication of MAC

MAC was fabricated to model the airway ciliary motion in both physiological and pathological states. MAC was produced by modifying a micro-molding method described before (Zhang et al., 2018) This method enables to control cilium shape and dimension and optimize magnetic particle distribution across the length of each cilium, thus the control of dynamic parameters influencing mucus propulsion. The details can be found in Supporting information 1—fabrication of the MAC. Briefly, by applying photolithography, well-defined molds were made featuring arrays of cylindrical-shaped microwells with a diameter of 50 μm, a length of 310 μm, and a pitch distance of 350 or 450 μm (to control cilia density). The microwells covered an area of 10 mm × 4 mm = 40 mm^2 containing 679 or 428 wells in case of 350 or 450 μm pitch, respectively. A magnetic precursor mixture made of PDMS and 5 μm magnetic microparticles (MMPs) was prepared in a 1:2 PDMS:MMP ratio. This precursor was poured over the mold in a vacuum environment to fill the microwells. Once finished, the excess PDMS:MMP outside the microwells was removed, pure PDMS was poured into the mold, and the structure was then spin-coated to obtain a pure PDMS layer with a thickness of approximately 100 μm. The so formed structure was then left in an oven to cure at 100°C for 3 h with a permanent magnet underneath the mold. This magnet imposes MMP alignment along the cilia length due to the magnetic field. Finally, the MAC was carefully peeled off the mold. Hence, MAC was obtained standing on a transparent nonmagnetic PDMS base substrate.

2.4 | Magnetic actuation of the MAC

The created MAC can be actuated by applying an external magnetic field. Thanks to the aligned MMPs within each cilium, the MAC tend to align themselves with the magnetic field. It was previously demonstrated that the MAC can be actuated to exhibit synchronous rotation along a tilted cone by using a rotating magnet (Zhang et al., 2019). Here, we use the method introduced by Zhang et al. (2020) to generate metachronal motion in which each of the individual MAC exhibits the oscillatory motion that resembles that of airway cilia (Zhang et al., 2020). The metachronal motion is realized with a home-built novel magnetic actuation setup, which consists of an array of rod-shaped permanent magnets that are arranged to have alternating dipole orientation between consecutive magnets (Figure S1a). This configuration of magnets generates a nonuniform, but periodic magnetic field (Figure S2a), resulting in a phase difference between the beatings of adjacent MAC as each cilium tends to align its long axis with the applied local magnetic field, and thus the MAC array exhibits a metachronal wave (Zhang et al., 2020). This setup is termed "magnet-belt." The rod-shaped magnets have a diameter of 4 mm and a length of 10 mm, and they have a remnant magnetic flux density of 1.2T.

2.5 | Characterization of the MAC

The overall shape, diameter, length, pitch, and magnetic particle distribution were characterized through optical microscopy (KEYENCE VHX-5000). The MAC motion resulting from the magnet-belt actuation was characterized by taking high-speed image sequences at a frame rate of 2000 fps using a high-speed camera (Phantom V9.0; Vision Research) mounted on a microscope (Olympus SZ61). These high-speed images were later analyzed with ImageJ using the tool *Manual tracking* to identify cilium tip speed along the entire beating cycle.

To study the ability of the cilia to generate net flows with a free boundary, an annular poly(methyl methacrylate) (PMMA) channel (Figure S1b) of 6-mm height and 10-mm width was exploited. The ciliated mat (10 mm × 4 mm) was positioned in the channel and submitted to plasma treatment (Tantec HF SpotTEC) to render its surface hydrophilic. After treatment, water containing 8 μm polystyrene particles (COOH surface; Micromer-blue), referred to as tracking particles, were used to characterize fluid propulsion. MAC with different pitches (350 and 450 μm) was actuated by the magnet belt at a beating frequency of 10 and 1 Hz to replicate ciliary beating frequencies in physiological and CF conditions, respectively (Birket et al., 2014; Hill et al., 2014; Lum et al., 2007; Wilkens et al., 2010). Fluid propulsion was determined by analyzing the movement of the tracking particles present in the fluid. A defined amount of liquid filled in the channel was introduced to obtain different water levels, namely 3.8, 5.6, 7.5, and 9.4 ml to achieve a water height of 2, 3, 4, and 5 mm, respectively. Different water levels were evaluated to determine the correlation between water volume/height and particle speed. Particle movement at the geometrical center of the channel at the location indicated in Figure S1b was recorded using a CMOS camera (DFK 33UX252) mounted on a microscope (Olympus SZ61). These recorded images were analyzed using the Manual Tracking tool of *ImageJ*.

2.6 | Coupling of L-Mu^3Gel and MAC

To observe the transport of L-Mu^3Gel over MAC, the ciliated mat was integrated into the annular PMMA open channel with a height of 500 μm and a width of 10 mm (50 and 70 mm of internal and external diameter, respectively), which was filled with 950 μl of a PCL-simulant (either water or glycerol), resulting in a layer thickness of 500 μm. The thickness of the PCL-simulant layer was kept constant and proportional to the length of the MAC to reproduce physiological proportions. In spite of plasma treatment (Tantec HF SpotTEC) to render both channel and ciliated mat hydrophilic, PCL-simulant layer thickness had to be fixed at 500 μm to ensure its homogeneous

distribution across the channel. The L-Mu^{3}Gel was then deposited over the PCL-simulant, and MAC was actuated by the magnet belt at 10 Hz to reproduce physiological ciliary beating (Hill et al., 2014; Lum et al., 2007; Wilkens et al., 2010). The movement of the L-Mu^{3}Gel was recorded using the CMOS camera and later analyzed using *ImageJ* (*Manual Tracking* tool) by observing particle's position over time and, thus, computing their speed.

2.7 | Coupling of CF-Mu^{3}Gel and MAC

To reproduce the MCC in CF conditions, the PMMA annular open channel, within which a ciliated mat was located, was covered with CF-Mu^{3}Gel. A ciliary beating frequency of 1 Hz was introduced to reproduce the ciliary beating frequency in CF airways (Birket et al., 2014), and CF-Mu^{3}Gel motion was recorded. Later, the CF-Mu^{3}Gel was treated with 1 ml of 0.5 M sodium EDTA to reproduce CF mucus degradation by mucolytic action. EDTA action over CF-Mu^{3}Gel was recorded through microscopy and imaging analyses (*IC Capture 2.4* software). The resultant flow was evaluated using the *Manual Tracking* tool of *ImageJ* by observing particle's position over time to determine their speed.

2.8 | Statistical analyses

The reported results are presented as the mean of at least three independent experiments using Student's *t*-test and one-way analysis of variance in GraphPad Prism version 8 (GraphPad Software). The differences were considered significant if $p < 0.05$.

3 | RESULTS AND DISCUSSION

3.1 | L-Mu^{3}Gel as a model of physiological mucus

Like in human mucus, mucin is the major component of L-Mu^{3}Gel and its impact on the viscoelastic properties was investigated by selecting two concentrations of 2.0% and 5.0% (wt/vol) in 0.48% (wt/vol) sodium chloride, the range of concentrations reported for physiological airway mucus (Bansil et al., 1995; Henke et al., 2007). L-Mu^{3}Gel has a homogeneous structure that exhibited gel behavior characterized by viscoelastic properties similar to those of physiological mucus (Figure 2a). Overall, L-Mu^{3}Gel exhibited a G' of 0.70–1.6 Pa and a G'' of 0.59–1.4 Pa in the frequency range of 0.1–20 Hz (Figure 2c,d). The viscoelastic properties of L-Mu^{3}Gel were comparable to those of physiological airway mucus that exhibits a G' between 0.75 and 2.1 Pa and a G'' between 0.27 and 0.80 Pa in the same frequency range (Yuan et al., 2015). A higher concentration of mucin of 5.0% (wt/vol) resulted in increased G' and G'', but with respect to L-Mu^{3}Gel composed of 2.0% (wt/vol) mucin, the differences were not significant and both concentrations reproduced the viscoelastic behavior of physiological airway mucus.

Mucus is known to exhibit a crosslinked structure in which the degree of mucin entanglements defines a mesh size that, in turn, determines mucus viscoelastic characteristics and impacts the diffusion of different molecules through its structure. To get further insights into the structure of L-Mu^{3}Gel, the generalized Maxwell model was fitted to the rheological data to determine the elastic modulus of the fully relaxed material, G_∞, as the sum of the moduli characterizing the different relaxation modes (Figure 2e and Supporting Information 2). This, in turn, allowed the estimation of the mesh size of L-Mu^{3}Gel (Figure 2f) through the application of the rubber elasticity theory, assuming ideal rubber behavior, as previously reported (Pacheco et al., 2019; Turco et al., 2011). The estimated mesh size of L-Mu^{3}Gel varied between 90.3 and 112.2 nm (Figure 2f), which corresponds to the lower limit of the values reported for physiological airway mucus (Kirch et al., 2012; Schuster et al., 2013). The values compared well with those reported by Kirch et al. (2012) and Schuster et al. (2013). Yet, according to Suk et al. (2009), the mesh size of physiological mucus ranges between 497 and 503 nm (Suk et al., 2009). The differences among the data reported in the literature might be related to the methodology employed to determine the mesh size. Dehydration and fixation procedures used during electron microscopy preparations may alter mucus native microstructure (Suk et al., 2009). Based on the estimated mesh size values, L-Mu^{3}Gel may be used to analyze the permeability of smoke, pollutants, and bacteria, as well as drugs and particles and their effects on mucus properties.

3.2 | CF-Mu^{3}Gel as a model of CF mucus

CF-Mu^{3}Gel was adopted as a model of pathological mucus because it reproduces most features that directly affect mucus transport in CF airways, including composition, viscoelastic properties, gradient structure, and ability to support bacterial growth ("Www.Bac3Gel.Com"). CF-Mu^{3}Gel contains 2.5% (wt/vol) mucin and 0.71% (wt/vol) sodium chloride that falls within the ranges previously determined in CF sputum (Dodge, 2015; Henke et al., 2007; Matsui et al., 1998). Apart from the chemical composition, it was also considered that the viscoelastic properties of CF mucus vary not only between patients but also within a single patient in a short period of time (Nielsen et al., 2004; Radtke et al., 2018). Indeed, comparing the reported studies performed on CF sputum, G' may vary between 1 and 100,000 Pa, while G'' can range from 0.05 to 100,000 Pa (Bhat et al., 1996; Nielsen et al., 2004; Sriramulu et al., 2005; Stigliani et al., 2016; Suk et al., 2009). Thus, one mucus model is not able to model all variations at the same time, yet, as herein shown, the viscoelastic properties of CF-Mu^{3}Gel can be easily modified to take into account such variations (Figure 3a,b). CF-Mu^{3}Gel produced using either 0.16 or 0.30% (wt/vol) Ca^{2+} ions were used to represent different stages of disease progression that differently impact mucociliary transport in CF airways (Figure 3a,b). The viscoelastic properties of CF-Mu^{3}Gel fall within the range reported for CF sputum from different patients (Bhat et al., 1996; Nielsen et al., 2004; Sriramulu et al., 2005; Stigliani

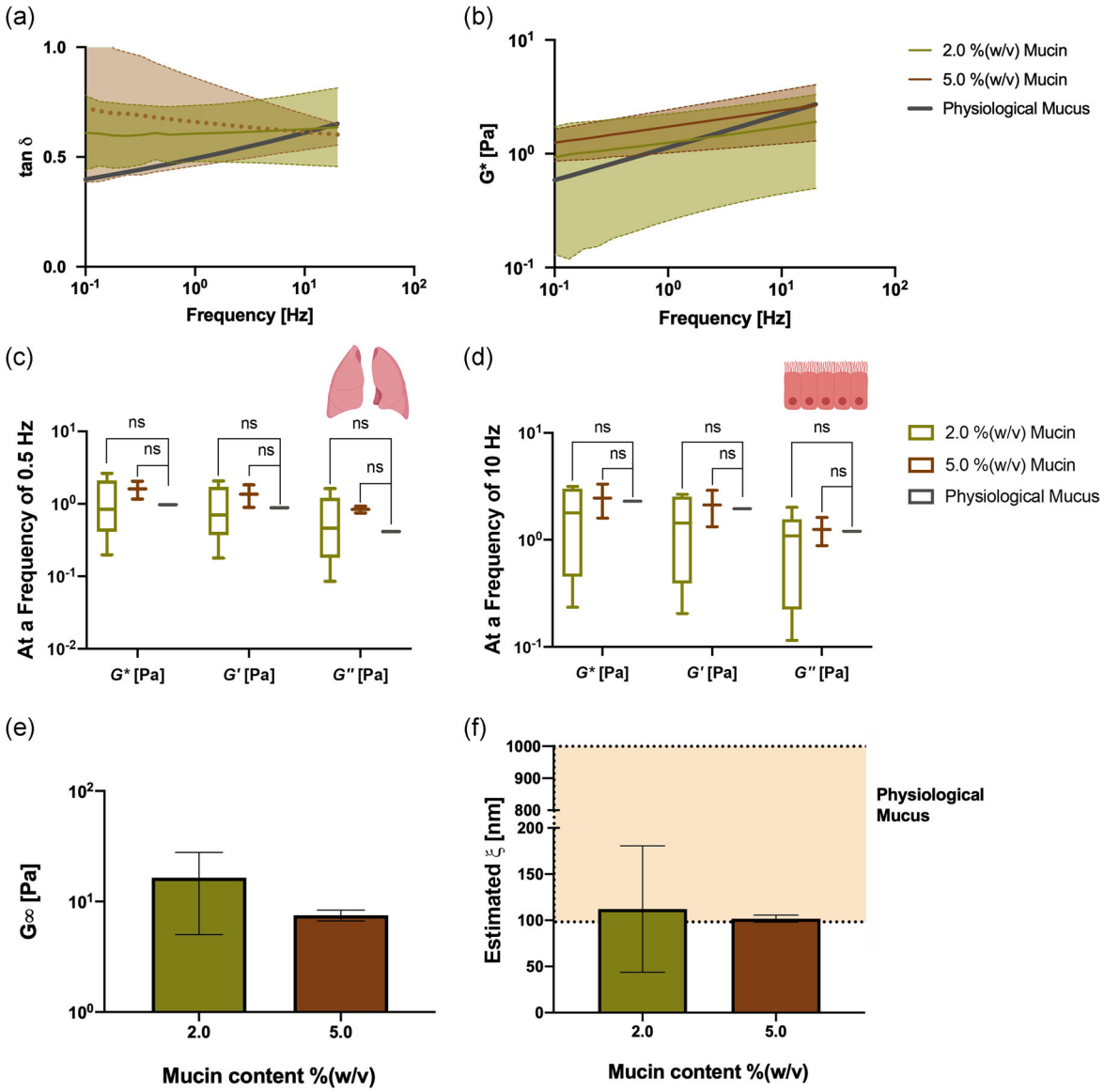

FIGURE 2 Viscoelastic properties and structural features of L-Mu^{3}Gel. (a–d) Rheological characterization in frequency sweep mode of L-Mu^{3}Gel using different mucin concentrations. The viscoelastic properties of physiological sputum are depicted as reported by (Yuan et al., 2015). (a) tan δ; and (b) complex modulus (G^*, Pa). G^* (Pa), G' (Pa), and G'' (Pa) at (c) breathing (~0.5 Hz); and (d) ciliary beating frequencies (~10 Hz). (e) Shear modulus of the fully relaxed material (G_∞); and (f) mesh size (ξ) of L-Mu^{3}Gel estimated by combining the GMM with the rubber elasticity theory. A minimum of three independent samples was analyzed per formulation ($n \geqq 3$). The area round the lines in (a) and (b), as well as the error bars in (e) and (f) represent the standard deviation. In (c) and (d) the bars correspond to maximum and minimum. In (f), the shadowed region depicts the range of mesh sizes reported in the literature for physiological airway mucus (Kirch et al., 2012; Schuster et al., 2013). (c) and (d) were analyzed using the one-way ANOVA test, while (e) and (f) were analyzed using the Student's *t*-test. No statistically significant differences were found in any comparison (*ns*). ANOVA, analysis of variance; GMM, generalized Maxwell model.

et al., 2016; Suk et al., 2009). A higher concentration of Ca^{2+} ions resulted in higher values of the viscoelastic properties for all tested formulations, as expected from the Ca^{2+}-induced crosslinking mechanism (Li et al., 2016; Moreira et al., 2014). This indicates that variations of Ca^{2+} concentration may be explored to match the viscoelastic properties of a wider number of CF patients and to possibly aid the development of patient-specific pharmacological treatments.

The mesh size of both types of CF-Mu^{3}Gel was also estimated to understand the effects of Ca^{2+} concentration on the microstructure (Figure 3c,d). As expected, higher Ca^{2+} concentration led to increased shear modulus of the fully relaxed material (Figure 3c) and decreased mesh sizes (Figure 3d). The estimated mesh sizes of CF-Mu^{3}Gel produced with 0.16% and 0.30% (wt/vol) Ca^{2+} ions were approximately 36.0 and 17.3 nm, respectively (Figure 3d). The mucus in patients with CF shows a reduced mesh size as compared to that

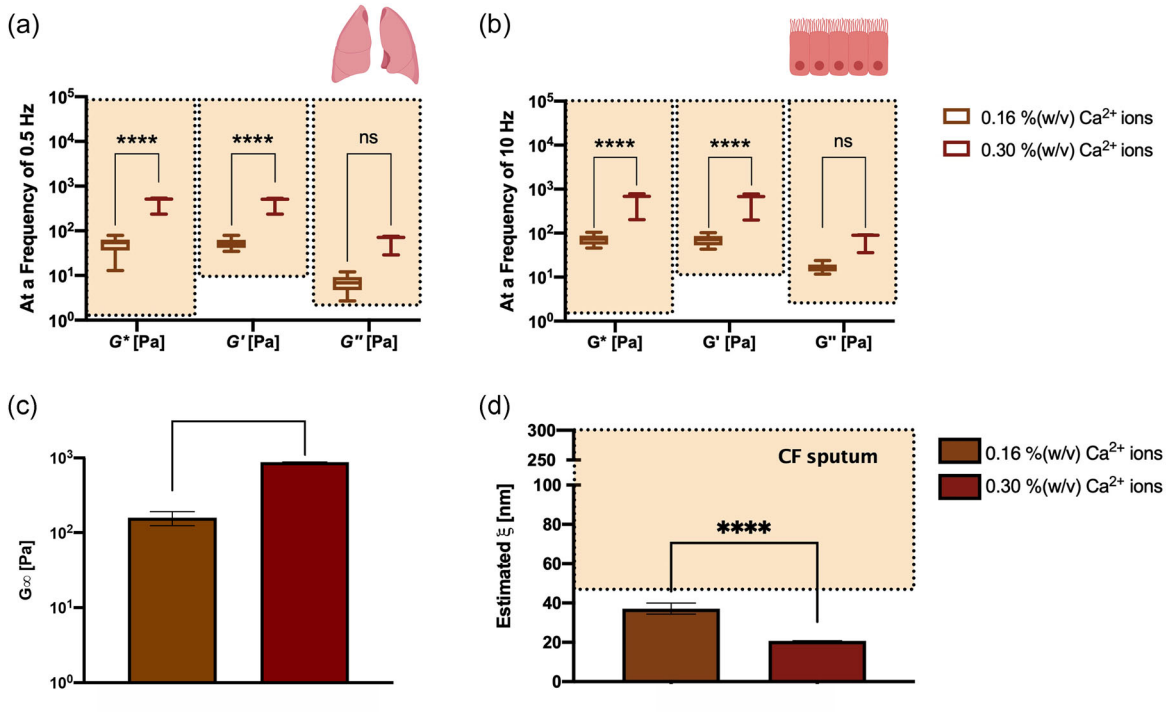

FIGURE 3 Viscoelastic properties and structural features of CF-Mu^{3}Gel. (a, b) Rheological characterization in frequency sweep mode of CF-Mu^{3}Gel produced using different Ca^{2+} concentrations containing 2.5% (wt/vol) mg/ml mucin, including G^* (Pa), G' (Pa) and G'' (Pa) at (a) breathing (~0.5 Hz); and (b) ciliary beating frequencies (~10 Hz). The obtained data are compared to the viscoelastic properties reported in the literature from the sputum of different CF patients (Bhat et al., 1996; Nielsen et al., 2004; Sriramulu et al., 2005; Stigliani et al., 2016; Suk et al., 2009). (c) Shear modulus of the fully relaxed material (G_∞); and (d) mesh size (ξ) of CF-Mu^{3}Gel estimated by combining the GMM with the rubber elasticity theory. Significant differences were set for $^*p < 0.05$; $^{**}p < 0.01$; $^{***}p < 0.001$; $^{****}p < 0.0001$, while *ns* corresponds to nonsignificant differences. A minimum of three independent samples were analyzed per formulation ($n \geqq 3$). In (a) and (b) the bars correspond to maximum and minimum, whereas in (c) and (d) represent the standard deviation. In (d), the shadowed region depicts the range of mesh sizes reported in the literature for pathological CF sputum (Suk et al., 2009). (a–d) were analyzed using the Student's *t*-test. CF, cystic fibrosis; GMM, generalized Maxwell model P.

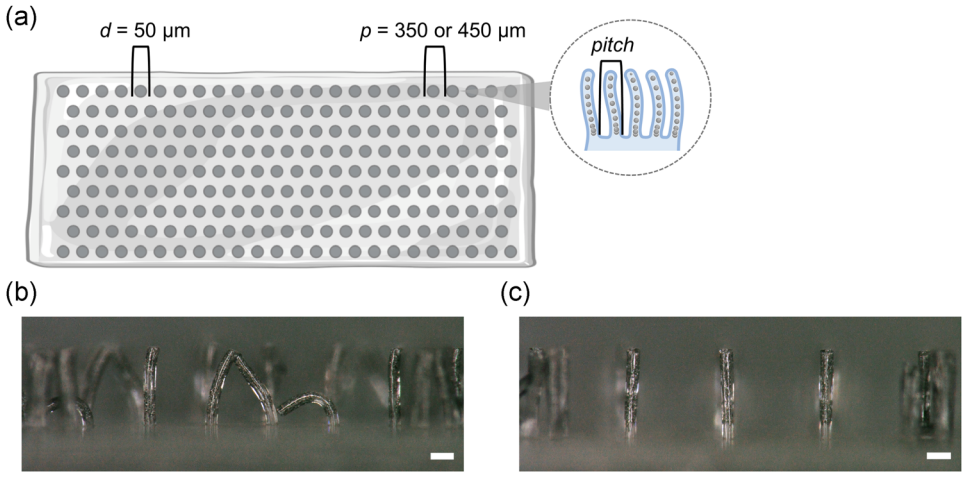

FIGURE 4 Magnetic artificial cilia (MAC) features. (a) Schematic representation of the staggered rearrangement of MAC aimed at increasing cilia density in the ciliated mat. (b, c) Micrographs of the fabricated MAC with (b) 200-μm pitch, depicting cilia adhesion between neighboring cilia; and (c) 350-μm pitch. The scale bars correspond to 100 μm.

of healthy patients (Figures 2f and 3d; Suk et al., 2009), a feature which is reproduced by CF-Mu^{3}Gel.

3.3 | MAC features

Human airway cilia have a diameter of 250 nm and a length of 7 μm (Henning et al., 2008), which corresponds to an aspect ratio of 28. Here, we have fabricated MAC with a cylindrical shape displaying a diameter of 50 μm and a height of 310 μm (Figure 4). Due to the intrinsic limitations of the exploited production method, it was difficult to achieve the dimensions of physiological cilia, even after optimizing all processing parameters (Supporting Information 1). Therefore, the MAC is substantially thicker and longer than human airway cilia, with a lower aspect ratio of 6.

Apart from single cilium characteristics, their placement in the ciliated mat plays a crucial role. Human ciliary density is approximately 8 cilia/μm^2 (Henning et al., 2008). To increase cilia density in the ciliated mats, while still preventing cilia attachment to the neighboring ones, a staggered arrangement in a rectangular grid was employed (Figure 4a). In this way, a cilia density of either 1.69×10^{-5} or 1.07×10^{-5} cilia/μm^2 was obtained when the ciliated mats presented 350- or 450-μm pitch, respectively. The obtained densities were limited by the minimum achievable pitch of 350 μm (Figure 4c), since lower pitch values resulted in cilia adhesion, either between neighboring cilia or between cilia and substrate (Figure 4b). By recalculating the density values into areal coverages, a value of 3.1×10^{-4} is obtained for the in vivo conditions, whereas this amounts to either 5.6×10^{-2} or 3.5×10^{-2} for MAC holding 350- or 450-μm pitch, respectively (Table S1).

The MAC is actuated by an external magnetic field, enabling an easy control of frequency at which these beat to match the ciliary beating frequency of physiological (10 Hz; Hill et al., 2014; Lum et al., 2007; Wilkens et al., 2010) and CF (1 Hz) states (Birket et al., 2014). Being so easily controllable, this enables to have a customizable model that is highly reproducible and that does not require cell culture. The force exerted by the cilium tip is also of relevance because the balance between the applied force and the hydrodynamic resistances will determine the actual trajectory followed by the cilia and hence fluid flow and mucus transport. In vivo, ciliary forces of 8.00×10^{-4} μN per cilium have been reported (Droguett et al., 2017), whereas in our case each cilium exerts a magnetic force of 12.7 μN. Hence, considering a ciliated area of 1 μm^2, this results in a value of 6.40 nN in vivo versus that of the ciliated mat herein proposed of about 0.210 and 0.136 nN with a pitch of 350 and 450 μm, respectively.

Since neighboring cilia adhere to each other and to the substrate when they are too close to each other (Figure 4b), it is difficult to meet native human cilia density. However, this parameter was compensated by the force exerted by each artificial cilium, which is much higher than the one exerted by physiological airway cilia. In fact, the lower density of the proposed ciliated mat with respect to physiological airway cilia resulted in a force generated per μm^2 of the same order of magnitude as for human airway cilia. Yet, future improvements may enable a more accurate reproduction of cilia dimensions and density by eventually exploiting nonsticky materials, such as thiol-ene polymers (Carlborg et al., 2011).

3.4 | Ciliary beating and metachronal wave

The MAC array is actuated by a magnet-belt to exhibit a metachronal wave (Figures 5d,e and S1), while each individual cilium performs a two-dimensional (2D) whip-*like* motion (Figure 5a–c) that is similar to the ciliary beating features of airway cilia (Elgeti & Gompper, 2013; Mitran, 2007). By controlling the external magnetic field, it was possible to control ciliary beating frequency. The 2D motion is composed of an effective (elastic) stroke when the cilium beats in the same direction as the traveling metachronal wave (Figure 5b), and a recovery (magnetic) stroke when the cilium mostly follows the applied magnetic field and moves in the opposite direction with respect to the traveling metachronal wave (Figure 5c). This motion reproduces that of physiological human airway cilia, characterized by a two-phase movement related to ATP consumption, asymmetric in space, time, and phase between each cilium (Droguett et al., 2017). In this study, the elastic, magnetic, and sliding strokes described by Zhang et al. (2020) were termed effective (elastic) and recovery (magnetic and sliding) strokes, which are commonly employed to describe human airway cilia motion (Figure 5a–c). Since the majority of literature studies regarding human airway cilia report a two-phase movement composed of an effective and a recovery stroke (Khelloufi et al., 2018; Raidt et al., 2014; Sedaghat et al., 2016), the so-called "sliding stroke" reported by Zhang et al. (2020) was considered as embedded in the magnetic stroke in one single phase and designated to be part of the recovery stroke (Zhang et al., 2020). With respect to the initial vertical position, the cilium whips from −24° to +76° during the effective stroke (Figure 5b), and passes back from +76° to −24° during the recovery stroke (Figure 5c). These values are slightly different with respect to those obtained by Zhang et al. (2020), who reported oscillations from +66° to −14°, which is probably associated with the difference in cilia height since the cilia adopted herein are 40 μm shorter (Zhang et al., 2020). The effective stroke is faster than the recovery stroke, indicated by the lower amount of image sequences within the same time interval in Figure 5b compared to Figure 5c. A quantitative analysis of both strokes revealed that the effective stroke constituted less than 1% of the entire beating cycle (Figure 5b), whereas the recovery stroke comprised up to 99% of the cycle (Figure 5c), in agreement with previous results (Zhang et al., 2020). In physiological conditions, the effective and recovery strokes occupy 20% and 80% of a single beating cycle, respectively (Vasquez & Forest, 2015). In comparison to the MAC, the effective stroke in human airway cilia takes a longer time. These differences are probably related not only to the different lengths and diameters between physiological airway cilia and MAC but also to the magnetic actuation. By scaling the MAC, by varying the magnetic actuation speed, the geometrical design of the magnet-belt and/or the disposition of the magnetic particles across the length of a single cilium, it would be

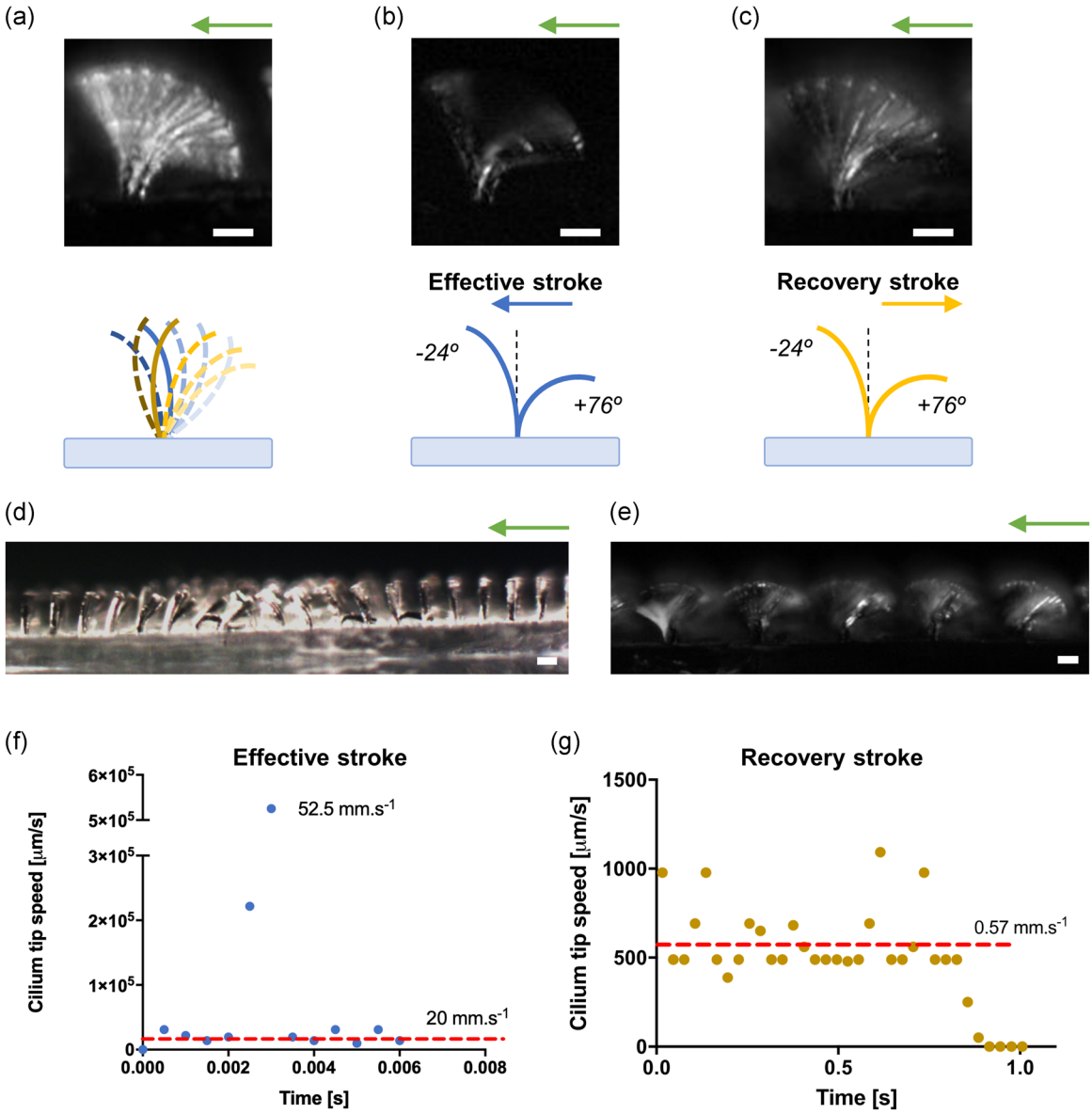

FIGURE 5 Features of the magnetic artificial cilia (MAC) motion and the metachronal wave generated by magnetic actuation. (a–c) Overlapping high-speed micrographs of a single cilium (top) and the corresponding schematic representation (bottom) during (a) a complete beating cycle; (b) effective (elastic) stroke; and (c) the recovery (magnetic) stroke at a beating frequency of 10 Hz. (d, e) MAC positioned over a magnet-belt under the microscope: (d) Micrograph of the ciliated mat positioned 1.1 mm above the surface of the rod-shaped magnets of the magnet belt, exhibiting a metachronal wave; and (e) overlapping of high-speed micrographs to show cilia movement over one beating cycle; the green arrows indicate the metachronal wave traveling direction. (a–e). The scale bars correspond to 100 μm. The effective (elastic) and recovery (magnetic) strokes are depicted in blue and yellow, respectively. (d, e) The direction of the metachronal wave is indicated by a green arrow. (f, g) Cilium tip speed during (f) effective and (g) recovery strokes at a beating frequency of 1 Hz. The horizontal red dash lines in (f) and (g) indicate the average tip speed.

possible to increase the effective stroke duration and thus to decrease the duration of the recovery stroke.

The effective stroke can be classified into three beating stages in terms of cilia tip speed: The first one is from +76° to +56° during which the average cilia tip speed is 20 mm/s; the second one is from +56° to −22° during which the maximum tip speed is reached (525 mm/s); and the third one is from −22° to −24° with a mean tip speed of 20 mm/s (Figure 5f). In contrast, during the recovery stroke, the average cilia tip speed is only 0.57 mm/s, with a maximum speed of nearly 1 mm/s (Figure 5g). Physiologically, cilium tip speed during the effective stroke is reported to range from 0.3 to 1 mm/s (Sears et al., 2013; Vasquez & Forest, 2015), whereas during the recovery stroke it is around 0.2 mm/s (Sears et al., 2013). The tip speed of MAC during the effective stroke is higher than the range reported in the literature, whereas the average MAC tip speed during the recovery stroke is comparable with the physiological one, having the

same order of magnitude. These differences might be related to MAC different dimensions and stiffnesses with respect to physiological ones, as well as to the specifics of the magnetic actuation.

In addition to each cilium following a similar effective-recovery stroke movement, neighboring MAC was actuated so to move in an out-of-phase manner, thanks to the configuration of the magnets in the magnet-belt (Figure S1). This movement was asymmetric in phase, but coordinated, so that a 2D metachronal wave traveled over the MAC tips along the entire ciliated mat (Figure 5d,e). Similarly, in vivo, cilia beat out-of-phase to generate the so-called metachronal wave, considered to be responsible for mucus transport. In this model, this wave had a wavelength of approximately 4 mm, directly related to the 4-mm diameter of the magnets (Video S1). This is significantly higher than that of physiological cilia that varies between 20 and 40 μm (Vasquez & Forest, 2015). The use of smaller magnets within the magnet belt may be attempted to reduce the wavelength, as this was mostly determined by their dimension so that an in-scale model can be generated.

3.5 | Fluid flow generation by MAC

Fluid flow generated by MAC was characterized using an open annular channel to reproduce the air–liquid interface present in human airways. To do so, tracking particles were mixed in water and the channel was filled with different volumes (different water heights) to determine its impact on fluid flow. A substantial net flow was generated in the effective stroke direction, which is also the direction of the metachronal wave. Higher water volume resulted in lower particle tracking speed, which was more visible at a higher ciliary beating frequency (Figure S3 and Videos S2 and S3). This fact was independent of cilia density, as small variations were noticed for ciliated mats with different pitches (Figure S3). A more in-depth analysis of the flow generation properties of the MAC in a closed channel can be found in (Zhang et al., 2020).

3.6 | Engineering cell-free models of mucociliary transport

To create microphysiological and micropathological models of MCC, both L-Mu^{3}Gel (model of physiological mucus) and CF-Mu^{3}Gel (model of CF mucus) were coupled to the fabricated MAC. These modular airway models reproduce different characteristics of MCC phenomena and may pave the way to deepen our knowledge of its complex workings.

3.7 | Fully modeling the physiological mucociliary transport

L-Mu^{3}Gel was placed onto MAC and submitted to a ciliary beating frequency of 10 Hz to reproduce physiological mucociliary transport

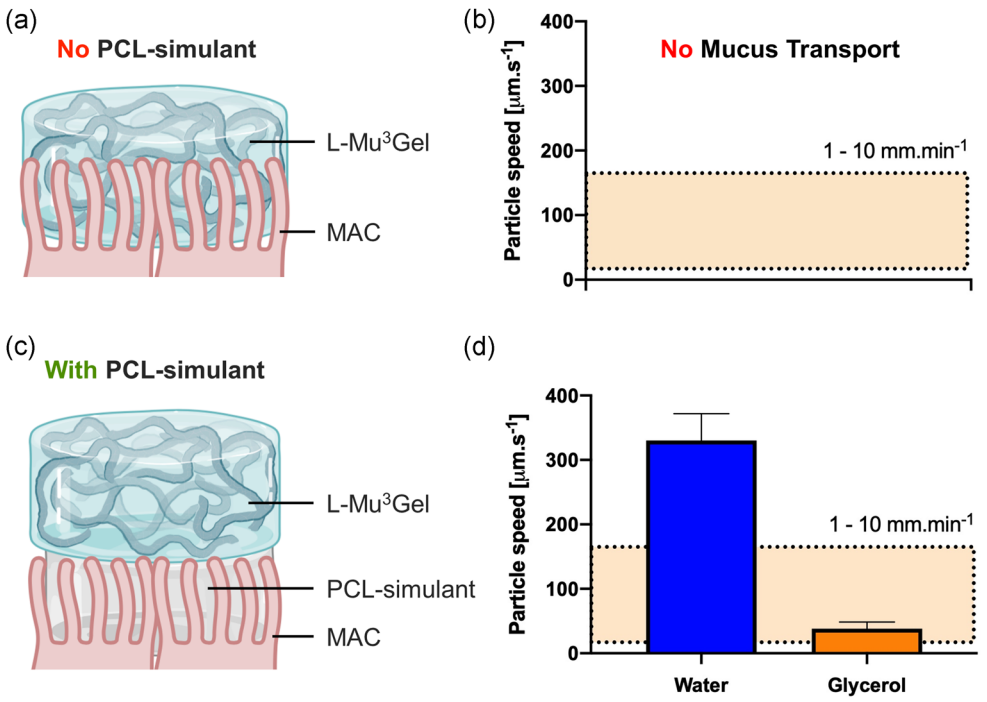

FIGURE 6 Microphysiological model of mucociliary transport characteristic of upper and large human airway surfaces. (a) Schematic representation of L-Mu^{3}Gel directly deposited over magnetic artificial cilia (MAC)—this is commonly observed in airway diseases; which leads to (b) stagnation of the mucus over the airway cilia. (c) Schematic representation of L-Mu^{3}Gel deposited over MAC in the presence of an intermediate periciliary layer (PCL)-simulant either water or glycerol; and (d) the resultant speed at which L-Mu^{3}Gel is transported at a ciliary beating frequency of 10 Hz. The shadowed region depicts the range of the reported speed at which physiologic mucus is propelled by the action of airway cilia (Cone, 2009; Vasquez & Forest, 2015).

(Hill et al., 2014; Lum et al., 2007; Wilkens et al., 2010). Different methods to combine the L-Mu^{3}Gel with MAC were implemented. First, L-Mu^{3}Gel was introduced directly over the ciliated area (Figure 6a). Even though cilia were able to move, they were not able to propel the L-Mu^{3}Gel, as the exerted force was not sufficient to overcome the friction with the bottom wall Video S4). The aggregates of tracking particles were immobile even after 60 s of ciliary beating. This is commonly observed in patients with either inherited or acquired airway diseases, as CF, COPD, and asthma (Button et al., 2012). Alternatively, a PCL-simulant was introduced between the MAC and L-Mu^{3}Gel to simulate the role of physiological PCL in the airways (Figure 6b). Given that the chemical composition and viscosity of the PCL are not known (Button et al., 2012; Cai, 2012), water was adopted as PCL-simulant. Taking inspiration from the physiological MCC, water was inserted so that its thickness was close (500 μm) to that of the MAC (310 μm), to replicate the human proportion of cilia (7 μm) to PCL (7 μm), while ensuring that it was homogeneously distributed through the fluidic chamber (Henning et al., 2008). Since the density of L-Mu^{3}Gel is similar to that of water (Figure S4), L-Mu^{3}Gel was able to float over the PCL-simulant. The speed at which L-Mu^{3}Gel was propelled was determined using nonmagnetic tracking particles present within the L-Mu^{3}Gel (Figure 6b). At 10 Hz, the L-Mu^{3}Gel moved at an average speed of 330 μm/s (Figure 6d and Video S5), which was lower than that determined in the absence of L-Mu^{3}Gel (1240 μm/s; Figure S3). To understand the effect of PCL-simulant viscosity and density on the overall mucociliary transport, glycerol was also introduced as an alternative PCL-simulant, which density is higher than that of L-Mu^{3}Gel (Figure S4). When glycerol was adopted as PCL-simulant, L-Mu^{3}Gel was propelled at a speed of 38.2 μm/s (Figure 6c and Video S6), which falls within the range of the reported speeds at which physiological mucus is propelled by airway cilia (Cone, 2009; Vasquez & Forest, 2015).

The different speed at which L-Mu^{3}Gel was propelled is related to the different viscosities of the PCL-simulants since the dynamic viscosity of water and glycerol is 1.001 and 1412 mPa·s, respectively. This results in a local Re higher than 1 when water is adopted as PCL-simulant, and thus inertia dominates and fosters the propulsion of L-Mu^{3}Gel. This is not observed when glycerol was adopted as PCL-simulant. The speed of mucus transport in physiological conditions is closer to that obtained when adopting glycerol as PCL-simulant than when water was employed. Differences between the in vitro setup and the in vivo condition can support the observed differences in mucus transport speed. Yet, it is worth to note that some studies report that tethered mucins and heparin sulfate can be found within the PCL and, probably, their presence causes an increase in the dynamic viscosity of the layer (Button et al., 2012; Cai, 2012), resulting in a viscosity higher than that of water. The modular character of the proposed physiological MCC model allows to easily modify the composition of the PCL-simulant to meet the composition of physiologic PCL, once this is defined, to create an even more realistic microphysiological model. It should be noted that in the proposed model, L-Mu^{3}Gel propulsion follows an antipletic metachronal wave that is, its flow follows the direction of the recovery stroke, which has been reported as the more efficient transport in human airway mucus than when the wave is symplectic that is, towards the effective stroke (Chateau et al., 2019).

The walls of the annular chamber used to characterize fluid propulsion are opaque and did not allow a direct evaluation of the position of L-Mu^{3}Gel over MAC and, thus, the Archimedes' principle was exploited (Supporting Information 3). Considering water as PCL-simulant and L-Mu^{3}Gel as a perfect prism of volume V' equal to 1.37 mm^3 (given its density of 773 mg/ml; Figure S2) and an overall volume of 1.73 mm^3, the submerged height was 541 μm. Following the same reasoning, the L-Mu^{3}Gel submerged height would be 429 μm in glycerol. It should be noted that these values are just a rough estimate because the soft nature of L-Mu^{3}Gel allows them to adapt their shape to the structure over which they are laid. Since the height of the PCL-simulant was set at 500 μm with respect to the base of the MAC and since the computed submerged heights are close to this value, it is probable that MAC comes into direct contact with L-Mu^{3}Gel (Figure 7b). Further investigations should be conducted using transparent annular channels that allow side view observations of the position of L-Mu^{3}Gel over the MAC and their arrangement. From a hydrodynamic point of view, the immersed

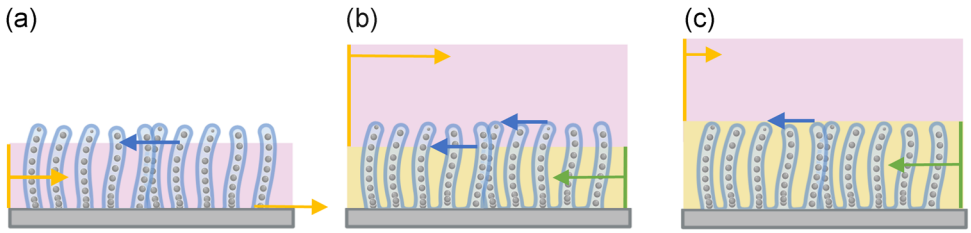

FIGURE 7 Proposed mechanisms for L-Mu^{3}Gel transport by the action of the magnetic artificial cilia (MAC). (a) L-Mu^{3}Gel is in direct contact with MAC and the underlying substrate and, as it happens in different airway diseases, no mucus propulsion is observed. (b) L-Mu^{3}Gel lays over the periciliary layer (PCL)-simulant, yet it comes into contact with MAC, as observed in physiological airways. (c) L-Mu^{3}Gel is barely in contact with the MAC tip. If transport is observed, this is associated with PCL-simulant transport in combination with the direct action of MAC. Pink and yellow represents L-Mu^{3}Gel and PCL-simulant, respectively. The blue structures depict the MAC. The blue arrow represents the effective stroke. The yellow arrow denotes the direction of L-Mu^{3}Gel transport, while the green arrow depicts the direction to which the PCL-simulant is propelled.

height of L-Mu^{3}Gel is expected to entail two counter-acting effects during mucus transport. First, a larger submerged height will result in a larger contact area between cilia and L-Mu^{3}Gel, which may improve the transfer of the actuation force between them. On the other hand, it results in a lower speed at the bottom surface of the L-Mu^{3}Gel, which reduces the propulsion speed. Moreover, in our case, where L-Mu^{3}Gel covers a limited surface area, additional body hydrodynamic resistance comes into play. However, this is absent in case a continuous mucus layer is present, as in physiological situations.

Apart from hydrodynamic resistance, L-Mu^{3}Gel transport over the MAC is determined by the force exerted by cilia, which is the driving force for mucus transport. In spite of a lower ciliary density of the MAC exploited in this study, the overall support of the L-Mu^{3}Gel by the cilia is definitely guaranteed (Figure S4). From Figure 7, it can be established that the force transfer can either occur in a direct way (Figure 7b) or partially (Figure 7c) via the hydrodynamics of the PCL. However, in the situation of Figure 7b, the L-Mu^{3}Gel may hinder cilia motion, as their bending would result in a shear motion inside the L-Mu^{3}Gel, whereby the ratio of L-Mu^{3}Gel stiffness as compared to bending stiffness of the cilia will determine the actual deformation and transport. It can be concluded that even though our microphysiological model adequately includes the relevant phenomena occurring in physiological conditions, significant challenges lay ahead to quantitatively model some of the in vivo features. However, rather than quantitatively mimicking in vivo conditions, the here proposed modular approach aims at providing the possibility to systematically vary the relevant parameters and thereby to investigate and pinpoint the dominant contributions under various conditions. The developed insights are indispensable for the development of novel therapeutic strategies.

3.8 | Fully modeling the CF mucociliary transport

In CF, mucociliary transport is hampered due to the presence of thick and sticky mucus and PCL depletion. Cilia bend downward onto the airway epithelium under the pathological mucus and, thus, they are not able to move and beat only up to a frequency of 1 Hz (Birket et al., 2014). To reproduce CF MCC, CF-Mu^{3}Gel was directly deposited over MAC (Figure 8a). As in pathological conditions, the presence of CF-Mu^{3}Gel caused MAC deformation underneath it, which hampered cilia motion (Video S7). Cilia were not able to fulfill an entire beating cycle or to even move (Figure 8b), resembling ciliary beating in CF airways where mucus transport is negligible (Birket et al., 2014).

Mucolytics are routinely administered to CF patients to reduce mucus viscoelastic properties, thus to improve mucociliary transport (Bhagirath et al., 2016; Bucki et al., 2015; Henke & Ratjen, 2007). The degradation of pathological mucus by the action of mucolytics was reproduced using sodium EDTA to degrade CF-Mu^{3}Gel (Figure 8a). EDTA is a chelating agent able to form four or six bonds with transition metal ions and/or main-

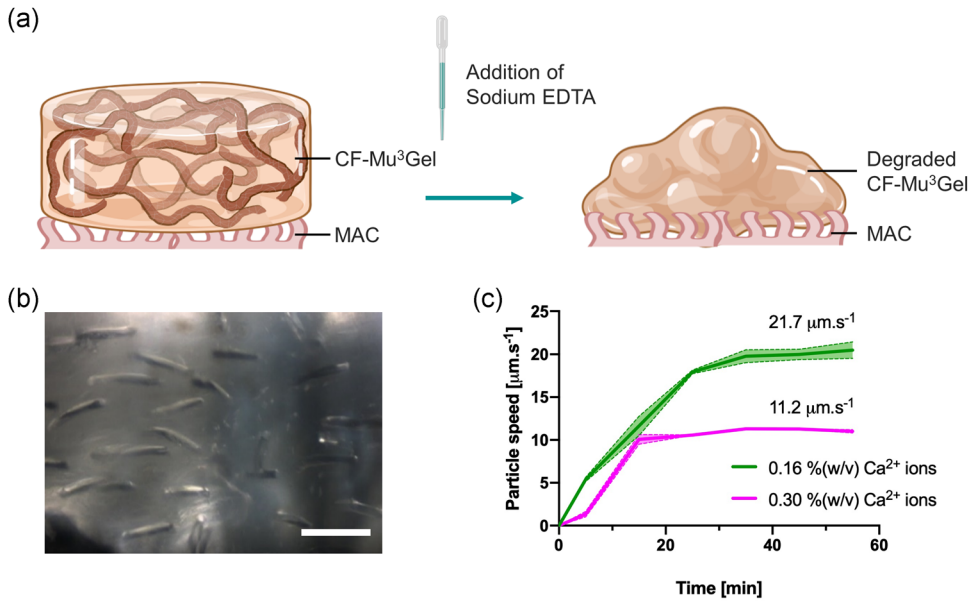

FIGURE 8 Micropathological model of mucociliary transport of CF airways. (a) Schematic representation of CF-Mu^{3}Gel coupled to MAC before and after the action of sodium EDTA. (b) Micrograph of CF-Mu^{3}Gel over MAC, which is compressed by the presence of CF-Mu^{3}Gel. The scale bar corresponds to 310 μm. (c) Particle speed inside the degraded CF-Mu^{3}Gel (8-μm polystyrene particles with COOH surface) as a function of both time of action of sodium EDTA and Ca^{2+} concentration, at a ciliary beating frequency of 1 Hz. The area round the lines represents the standard deviation. CF, cystic fibrosis; EDTA, ethylenediaminetetraacetic acid; MAC, magnetic artificial cilia.

group ions, usually bi- or trivalent, such as Ca^{2+} and Fe^{3+} ions (Mohammadi et al., 2013). In clinics, it is widely used as an antidote for lead, cadmium and/or iron poisoning, to prevent coagulation by sequestering the Ca^{2+} ions needed for clotting. Herein, sodium EDTA was used to recall the Ca^{2+} ions present in CF-Mu^{3}Gel, which resulted in a gradual rupture of pre-established crosslinks, thus reducing the viscoelastic properties (Figure 8a and Video S8). Briefly, CF-Mu^{3}Gel was applied over MAC and 1 ml of 0.5 M sodium EDTA was then directly poured over the CF-Mu^{3}Gel. Similar to what was previously reported, it promoted the gradual transition from solid to liquid-*like* state (Mahdi et al., 2016), enabling the transport of CF-Mu^{3}Gel by the action of MAC (Figure 8c). Within 5 min, the treated CF-Mu^{3}Gels started to be propelled, but a totally developed flow was only achieved after 20–25 min. After this period, a plateau was reached, indicating that the treated CF-Mu^{3}Gels had been degraded by the action of EDTA. When the plateau was reached, a flow speed of less crosslinked CF-Mu^{3}Gel (0.16% (wt/vol) Ca^{2+} ions) of nearly 20 μm/s was achieved, while more crosslinked CF-Mu^{3}Gel (0.30% [wt/vol] Ca^{2+} ions) reached only 11 μm/s. The different flow speeds reached at the plateau might be related to the viscosities of the degraded CF-Mu^{3}Gel that, in turn, are connected to the initial Ca^{2+} concentration. The average viscosity of CF-Mu^{3}Gel produced using 0.16% and 0.30% Ca^{2+} ions was 11.97 and 15.19 mPa·s, respectively after 20–25 min of sodium EDTA treatment (Figure 8c). Other calcium chelators or degradation agents may be used to promote the dissolution of CF-Mu^{3}Gel.

4 | CONCLUSIONS

In vitro models that address the complexity and dynamic conditions of the airway MCC apparatus may enable a better determination of the time of drug retention and elimination by the action of ciliary beating. Thereby, drug concentrations can be adjusted to guarantee maximum efficacy of pharmacological treatments before these being eliminated by the action of cilia propulsion towards the digestive system. With this in mind, microphysiological models of mucociliary transport in both physiological and CF states were engineered by coupling ad hoc mucus models with MAC.

L-Mu^{3}Gel and CF-Mu^{3}Gel with different chemical composition, viscoelastic properties, and structural features were tested, revealing that these can be easily modified according to pathology and disease progression in a patient-specific manner and with a structural transition resembling that of pathological mucus under the action of mucolytics. These models may be exploited as in vitro tools to determine the permeability of gases, pollutants, and drugs, as well as their effect on chemical composition and/or viscoelastic properties. Moreover, CF-Mu^{3}Gel may be useful to foster the development of new drugs during drug discovery or to ameliorate traditional ones, eventually providing patient-specific treatments to CF patients.

The MAC worked as micro-pumping hair-*like* systems that were able to beat once actuated by an external magnetic field. Indeed, upon external actuation, these structures move and, by tuning the motion of the magnet belt, it is possible to control flow direction and rate. MAC aspect ratio, dimension, and layout can be changed by varying the features of the mask during the production method and by selecting other materials. Thanks to the optimized distribution of magnetic particles within these cilia, their movement can be easily modified by changing the external magnetic field. The PCL-simulant can be changed in terms of height, chemical composition, and viscosity. The chemical composition of the PCL-simulant layer can be further changed to closely reproduce that of physiological and pathological PCLs, once their composition is determined.

The MCC models that we propose simultaneously consider the presence of cilia, PCL, and mucus, each one with characteristics that are easily modifiable in a reproducible manner. The fact that the models exclusively rely on readily available materials offers higher control over input parameters, as well as reproducible outcomes, which do not require specific equipment related to cell culture and complex characterization methods. Indeed, microscopic analyses together with *ImageJ* were the only tools adopted to investigate mucus transport.

In this study, we have developed a modular platform that models the MCC apparatus in vitro. The modular models are composed of different modules, each allowing independent variation of the various relevant parameters impacting mucociliary transport, and thus enabling the determination of the effect of each parameter and/or structure separately. The proposed modular concept offers several advantages with respect to current methods proposed for studying airway MCC since these are made of readily available materials, thus off-the-shelf, offer interlaboratory reproducibility, and can be easily customized to reproduce key features of different human airway disorders. Additionally, their versatility may be further exploited and adapted to produce in-scale models of airway MCC to closer reproduce airway clearance phenomena. Yet, the fabrication method adopted, in this study, to produce MAC is limited to the microscale, while nanofabrication has still to be developed. The integration of dimensional analysis may be another strategy to achieve dynamic similarity between the proposed in vitro model and the human airway system, by taking advantage of numerical analyses that have already been proposed to model ciliary dynamics (Vanaki et al., 2019) and MCC phenomena in both physiological and pathological states (Chatelin & Poncet, 2016; Chatelin et al., 2017; Sedaghat et al., 2016; Vanaki et al., 2020; Zhu et al., 2019). The proposed MCC model can, in turn, support numerical approaches in investigating how different ciliary features and configurations, as well as the composition and viscoelastic behavior of both PCL and mucus affect MCC and thus closely reproduce in silico airway human dynamics. In the future, our innovative approach can be exploited to study physiological and pathological MCC and possible treatments of the latter in a patient-specific and situation-specific manner.

ACKNOWLEDGMENTS

The authors thank Erwin Dekkers and Remco Felten of the TU/e Equipment & Prototyping Center for constructing the magnetic actuation setup. The schematic representations included in the manuscript were created with BioRender. com. Paola Petrini and Daniela Peneda Pacheco would like to thank the Switch2Product grant (UA.A.RRR.ARICID.SVRA.AUTO.AZ18VARI10) for partially funding the validation of the technology to be employed as airway models. Lucia Pedersoli acknowledges the Erasmus+ Program for the scholarship that enabled her to perform the internship at TU/e. Jaap den Toonder and Shuaizhong Zhang acknowledge funding from the European Research Council under the European Union's Horizon 2020 research and innovation program under grant agreement no. 833214.

CONFLICT OF INTERESTS

Daniela Peneda Pacheco is cofounder, shareholder, CTO at Bac^{3}Gel, Lda, a mucus-based company. Paola Petrini is cofounder, shareholder, scientific advisor at Bac^{3}Gel, Lda. Other authors declare that there are no conflict of interests.

AUTHOR CONTRIBUTIONS

Daniela Peneda Pacheco had the initial idea of the project. Paola Petrini and Daniela Peneda Pacheco have conducted the experimental design for the analyses of the mucus models. Lucia Pedersoli, Paola Petrini, Francesco Briatico-Vangosa, and Daniela Peneda Pacheco performed the rheological characterization and further analyses of the mucus models. Lucia Pedersoli, Ruth Cardinaels, and Daniela Peneda Pacheco have drawn the experimental design for coupling the mucus models with cilia and their characterization. Lucia Pedersoli, Shuaizhong Zhang, and Jaap den Toonder conceived the magnetic artificial cilia. Shuaizhong Zhang and Jaap den Toonder conceived the magnetic-belt actuation system. Lucia Pedersoli, Daniela Peneda Pacheco, and Ruth Cardinaels idealized the annular open chamber. Lucia Pedersoli, Shuaizhong Zhang, Ruth Cardinaels, Jaap den Toonder, and Daniela Peneda Pacheco performed and analyzed the magnetic actuation experiments. Lucia Pedersoli and Daniela Peneda Pacheco wrote the manuscript. All authors discussed the results, commented on the manuscript, and contributed to its final version.

DATA AVAILABILITY STATEMENT

The authors confirm that all data supporting the findings reported on this study are available within the article and its Supporting Information Material.

REFERENCES

Bansil, R., Stanley, E., & LaMont, J. T. (1995). Mucin biophysics. *Annual Review of Physiology*, *57*(1), 635–657. https://doi.org/10.1146/annurev.physiol.57.1.635

Benam, K. H., Villenave, R., Lucchesi, C., Varone, A., Hubeau, C., Lee, H. H., Alves, S. E., Salmon, M., Ferrante, T. C., Weaver, J. C., Bahinski, A., Hamilton, G. A., & Ingber, D. E. (2016). Small airway-on-a-chip enables analysis of human lung inflammation and drug responses in vitro. *Nature Methods*, *13*(2), 151–157. https://doi.org/10.1038/nmeth.3697

Bhagirath, A. Y., Li, Y., Somayajula, D., Dadashi, M., Badr, S., & Duan, K. (2016). Cystic fibrosis lung environment and *Pseudomonas aeruginosa* infection. *BMC Pulmonary Medicine*, *16*(1), 174. https://doi.org/10.1186/s12890-016-0339-5

Bhat, P. G., Flanagan, D. R., & Donovan, M. D. (1996). Drug diffusion through cystic fibrotic mucus: Steady-state permeation, rheologic properties, and glycoprotein morphology. *Journal of Pharmaceutical Sciences*, *85*(6), 624–630. https://doi.org/10.1021/js950381s

Birket, S. E., Chu, K. K., Liu, L., Houser, G. H., Diephuis, B. J., Wilsterman, E. J., Dierksen, G., Mazur, M., Shastry, S., Li, Y., Watson, J. D., Smith, A. T., Schuster, B. S., Hanes, J., Grizzle, W. E., Sorscher, E. J., Tearney, G. J., & Rowe, S. M. (2014). A functional anatomic defect of the cystic fibrosis airway. *American Journal of Respiratory and Critical Care Medicine*, *190*(4), 421–432. https://doi.org/10.1164/rccm.201404-0670OC

Bucki, R., Cruz, K., Pogoda, K., Eggert, A., Chin, L., Ferrin, M., Imbesi, G., Hadjiliadis, D., & Janmey, P.A. (2015). Enhancement of pulmozyme activity in purulent sputum by combination with poly-aspartic acid or gelsolin. *Journal of Cystic Fibrosis*, *14*(5), 587–593. https://doi.org/10.1016/j.jcf.2015.02.001

Button, B., Cai, L.-H., Ehre, C., Kesimer, M., Hill, D. B., Sheehan, J. K., Boucher, R. C., & Rubinstein, M. (2012). A periciliary brush promotes the lung health by separating the mucus layer from airway epithelia. *Science*, *337*(6097), 937–941. https://doi.org/10.1126/science.1223012

Cai, L.-H. (2012). *Structure and function of airway surface layer of the human lungs & mobility of probe particles in complex fluids*.

Carlborg, C. F., Haraldsson, T., Öberg, K., Malkoch, M., & Van Der Wijngaart, W. (2011). Beyond PDMS: off-stoichiometry thiol-ene (OSTE) based soft lithography for rapid prototyping of microfluidic devices. *Lab on a Chip*, *11*(18), 3136–3147. https://doi.org/10.1039/c1lc20388f

Chateau, S., Favier, J., Poncet, S., & D'Ortona, U. (2019). Why antiplectic metachronal cilia waves are optimal to transport bronchial mucus. *Physical Review E*, *100*(4), 1–9. https://doi.org/10.1103/PhysRevE.100.042405

Chatelin, R., Anne-Archard, D., Murris-Espin, M., Thiriet, M., & Poncet, P. (2017). Numerical and experimental investigation of mucociliary clearance breakdown in cystic fibrosis. *Journal of Biomechanics*, *53*, 56–63. https://doi.org/10.1016/j.jbiomech.2016.12.026

Chatelin, R., & Poncet, P. (2016). A parametric study of mucociliary transport by numerical simulations of 3D non-homogeneous mucus. *Journal of Biomechanics*, *49*(9), 1772–1780. https://doi.org/10.1016/j.jbiomech.2016.04.009

Cone, & R. A. (2009). Barrier properties of mucus. *Advanced Drug Delivery Reviews*, *61*, 75–85. https://doi.org/10.1016/j.addr.2008.09.008

Dodge, A. (2015). A millennial view of cystic fibrosis. *Developmental Period Medicine*, *XIX*(1), 9–13.

Droguett, K., Rios, M., Carreño, D. V., Navarrete, C., Fuentes, C., Villalón, M., & Barrera, N. P. (2017). An autocrine ATP release mechanism regulates basal ciliary activity in airway epithelium. *The Journal of Physiology*, *595*(14), 4755–4767. https://doi.org/10.1113/JP273996

Elgeti, J., & Gompper, G. (2013). Emergence of metachronal waves in cilia arrays. *Proceedings of the National Academy of Sciences of United States of America*, *110*(12), 4470–4475. https://doi.org/10.1073/pnas.1218869110

Fahy, J. V., & Dickey, B. F. (2010). Airway mucus function and dysfunction. *New England Journal of Medicine*, *363*, 2233–2247. https://doi.org/10.1056/NEJMra0910061

Harding, S. E. (1989). The macrostructure of mucus glycoproteins in solution. *Advances in Carbohydrate Chemistry and Biochemistry*, *47*, 345–381. https://doi.org/10.1016/S0065-2318(08)60417-5

Henke, M. O., John, G., Germann, M., Lindemann, H., & Rubin, B. K. (2007). MUC5AC and MUC5B mucins increase in cystic fibrosis airway secretions during pulmonary exacerbation. *American Journal of*

Respiratory and Critical Care Medicine, *175*(8), 816–821. https://doi.org/10.1164/rccm.200607-1011OC

Henke, M. O., & Ratjen, F. (2007). Mucolytics in cystic fibrosis. *Paediatric Respiratory Reviews*, *8*(1), 24–29. https://doi.org/10.1016/j.prrv.2007.02.009

Henning, A., Schneider, M., Bur, M., Blank, F., Gehr, P., & Lehr, C.-M. (2008). Embryonic chicken trachea as a new in vitro model for the investigation of mucociliary particle clearance in the airways. *AAPS PharmSciTech*, *9*(2), 521–527. https://doi.org/10.1208/s12249-008-9072-6

Hill, D. B., Long, R. F., Kissner, W. J., Atieh, E., Garbarine, I. C., Markovetz, M. R., Fontana, N. C., Christy, M., Habibpour, M., Tarran, R., Forest, M. G., Boucher, R. C., & Button, B. (2018). Pathological mucus and impaired mucus clearance in cystic fibrosis patients result from increased concentration, not altered pH. *European Respiratory Journal*, *52*(6):1801297. https://doi.org/10.1183/13993003.01297-2018

Hill, D. B., Vasquez, P. A., Mellnik, J., Mckinley, S. A., Vose, A., Mu, F., Henderson, A. G., Donaldson, S. H., Alexis, N. E., Boucher, R. C., & Forest, M. G. (2014). A biophysical basis for mucus solids concentration as a candidate biomarker for airways disease. *PLoS ONE*, *9*(2), e87681. https://doi.org/10.1371/journal.pone.0087681

Khelloufi, M. K., Loiseau, E., Jaeger, M., Molinari, N., Chanez, P., Gras, D., & Viallat, A. (2018). Spatiotemporal organization of cilia drives multiscale mucus swirls in model human bronchial epithelium. *Scientific Reports*, *8*(2447), 1–10. https://doi.org/10.1038/s41598-018-20882-4

Kirch, J., Schneider, A., Abou, B., Hopf, A., Schaefer, U. F., Schneider, M., Schall, C., Wagner, C., & Lehr, C. M. (2012). Optical tweezers reveal relationship between microstructure and nanoparticle penetration of pulmonary mucus. *Proceedings of the National Academy of Sciences of United States of America*, *109*(45), 18355–18360. https://doi.org/10.1073/pnas.1214066109

Li, J., Wu, Y., He, J., & Huang, Y. (2016). A new insight to the effect of calcium concentration on gelation process and physical properties of alginate films. *Journal of Materials Science*, *51*(12), 5791–5801. https://doi.org/10.1007/s10853-016-9880-0

Liu, L., Shastry, S., Byan-Parker, S., Houser, G., K Chu, K., Birket, S. E., Fernandez, C. M., Gardecki, J. A., Grizzle, W. E., Wilsterman, E. J., Sorscher, E. J., Rowe, S. M., & Tearney, G. J. (2014). An autoregulatory mechanism governing mucociliary transport is sensitive to mucus load. *American Journal of Respiratory Cell and Molecular Biology*, *51*(4), 485–493. https://doi.org/10.1165/rcmb.2013-0499MA

Livraghi, A., & Randell, S. H. (2007). Cystic fibrosis and other respiratory diseases of impaired mucus clearance. *Toxicologic Pathology*, *35*(1), 116–129. https://doi.org/10.1080/01926230601060025

Lorenzi, G., Böhm, G. M., Guimarães, E. T., Costa Vaz, M. A., King, M., & Saldiva, P. H. N. (1992). Correlation between rheologic properties and in vitro ciliary transport of rat nasal mucus. *Biorheology*, *29*(4), 433–440. https://doi.org/10.3233/BIR-1992-29406

Lum, S., Gustafsson, P., Ljungberg, H., Hülskamp, G., Bush, A., Carr, S. B., Castle, R., Hoo, A. F., Price, J., Ranganathan, S., Stroobant, J., Wade, A., Wallis, C., Wyatt, H., & Stocks, J., London Cystic Fibrosis Collaboration. (2007). Early detection of cystic fibrosis lung disease: Multiple-breath washout versus raised volume tests. *Thorax*, *62*, 341–347. https://doi.org/10.1136/thx.2006.068262

Mahdi, M. H., Diryak, R., Kontogiorgos, V., Morris, G. A., & Smith, A. M. (2016). In situ rheological measurements of the external gelation of alginate. *Food Hydrocolloids*, *55*, 77–80. https://doi.org/10.1016/j.foodhyd.2015.11.002

Matsui, H., Grubb, B. R., Tarran, R., Randell, S. H., Gatzy, J. T., Davis, C. W., & Boucher, R. C. (1998). Evidence for periciliary liquid layer depletion, not abnormal ion composition, in the pathogenesis of cystic fibrosis airways disease. *Cell*, *95*(7), 1005–1015. https://doi.org/10.1016/S0092-8674(00)81724-9

Mitran, S. M. (2007). Metachronal wave formation in a model of pulmonary cilia. *Computers & Structures*, *85*(11–14), 763–774. https://doi.org/10.1016/j.compstruc.2007.01.015

Mohammadi, Z., Shalavi, S., & Jafarzadeh, H. (2013). Ethylenediaminetetraacetic acid in endodontics. *European Journal of Dentistry*, *7*(1), S135–S142. https://doi.org/10.4103/1305-7456.119091

Moreira, H. R., Munarin, F., Gentilini, R., Visai, L., Granja, P. L., Tanzi, M. C., & Petrini, P. (2014). Injectable pectin hydrogels produced by internal gelation: pH dependence of gelling and rheological properties. *Carbohydrate Polymers*, *103*, 339–347. https://doi.org/10.1016/j.carbpol.2013.12.057

Murgia, X., Loretz, B., Hartwig, O., Hittinger, M., & Lehr, C.-M. (2018). The role of mucus on drug transport and its potential to affect therapeutic outcomes. *Advanced Drug Delivery Reviews*, *124*, 82–97. https://doi.org/10.1016/j.addr.2017.10.009

Nielsen, H., Hvidt, S., Sheils, C. A., & Janmey, P. A. (2004). Elastic contributions dominate the viscoelastic properties of sputum from cystic fibrosis patients. *Biophysical Chemistry*, *112*(2–3), 193–200. https://doi.org/10.1016/j.bpc.2004.07.019

Norton, M. M., Robinson, R. J., & Weinstein, S. J. (2011). Model of ciliary clearance and the role of mucus rheology. *Physical Review E*, *83*(1), 011921. https://doi.org/10.1103/PhysRevE.83.011921

Pacheco, D. P., Butnarasu, C. S., Briatico Vangosa, F., Pastorino, L., Visai, L., Visentin, S., & Petrini, P. (2019). Disassembling the complexity of mucus barriers to develop a fast screening tool for early drug discovery. *Journal of Materials Chemistry B*, *7*(32), 4940–4952. https://doi.org/10.1039/C9TB00957D

Radtke, T., Böni, L., Bohnacker, P., Fischer, P., Benden, C., & Dressel, H. (2018). The many ways sputum flows—dealing with high within-subject variability in cystic fibrosis sputum rheology. *Respiratory Physiology and Neurobiology*, *254*, 36–39. https://doi.org/10.1016/j.resp.2018.04.006

Raidt, J., Wallmeier, J., Hjeij, R., Onnebrink, J. G., Pennekamp, P., Loges, N. T., Olbrich, H., Häffner, K., Dougherty, G. W., Omran, H., & Werner, C. (2014). Ciliary beat pattern and frequency in genetic variants of primary ciliary dyskinesia. *European Respiratory Journal*, *44*(6), 1579–1588. https://doi.org/10.1183/09031936.00052014

Schuster, B. S., Suk, J. S., Woodworth, G. F., & Hanes, J. (2013). Nanoparticle diffusion in respiratory mucus from humans without lung disease. *Biomaterials*, *34*(13), 3439–3446. https://doi.org/10.1016/j.biomaterials.2013.01.064

Sears, P. R., Thompson, K., Knowles, M. R., & Davis, C. W. (2013). Human airway ciliary dynamics. *American Journal of Physiology-Lung Cellular and Molecular Physiology*, *304*(3), L170–L183. https://doi.org/10.1152/ajplung.00105.2012

Sears, P. R., Yin, W.-N., & Ostrowski, L. E. (2015). Continuous mucociliary transport by primary human airway epithelial cells in vitro. *American Journal of Physiology-Lung Cellular and Molecular Physiology*, *309*(2), L99–L108. https://doi.org/10.1152/ajplung.00024.2015

Sedaghat, M. H., Shahmardan, M. M., Norouzi, M., Jayathilake, P. G., & Nazari, M. (2016). Numerical simulation of muco-ciliary clearance: Immersed boundary-lattice Boltzmann method. *Computers and Fluids*, *131*, 91–101. https://doi.org/10.1016/j.compfluid.2016.03.015

Sriramulu, D. D., Lu, H., Lam, J. S., & Romling, U. (2005). Microcolony formation: A novel biofilm model of *Pseudomonas aeruginosa* for the cystic fibrosis lung. *Journal of Medical Microbiology*, *54*, 667–676. https://doi.org/10.1099/jmm.0.45969-0

Stigliani, M., Manniello, M. D., Zegarra-Moran, O., Galietta, L., Minicucci, L., Casciaro, R., Garofalo, E., Incarnato, L., Aquino, R. P., Del Gaudio, P., & Russo, P. (2016). Rheological properties of cystic fibrosis bronchial secretion and in vitro drug permeation study: The effect of sodium bicarbonate. *Journal of Aerosol Medicine and Pulmonary Drug Delivery*, *29*(4), 337–345. https://doi.org/10.1089/jamp.2015.1228

Suk, J. S., Lai, S. K., Wang, Y.-Y., Ensign, L. M., Zeitlin, P. L., Boyle, M. P., & Hanes, J. (2009). The penetration of fresh undiluted sputum

expectorated by cystic fibrosis patients by non-adhesive polymer nanoparticles. *Biomaterials*, *30*(13), 2591–2597. https://doi.org/10.1016/j.biomaterials.2008.12.076

Turco, G., Donati, I., Grassi, M., Marchioli, G., Lapasin, R., & Paoletti, S. (2011). Mechanical spectroscopy and relaxometry on alginate hydrogels: A comparative analysis for structural characterization and network mesh size determination. *Biomacromolecules*, *12*(4), 1272–1282. https://doi.org/10.1021/bm101556m

Vanaki, S. M., Holmes, D., Jayathilake, P. G., & Brown, R. (2019). Three-dimensional numerical analysis of periciliary liquid layer: Ciliary abnormalities in respiratory diseases. *Applied Sciences*, *9*(19), 4033. https://doi.org/10.3390/app9194033

Vanaki, S. M., Holmes, D., Saha, S. C., Chen, J., Brown, R. J., & Jayathilake, P. G. (2020). Muco-ciliary clearance: A review of modelling techniques. *Journal of Biomechanics*, *99*, 109578. https://doi.org/10.1016/j.jbiomech.2019.109578

Vasquez, P. A., & Forest, M. G. (2015). Complex fluids and soft structures in the human body. In S. E. Spagnolie (Ed.), *Complex fluids in biological systems* (1st ed., pp. 53–110). Springer.

Wilkens, H., Weingard, B., Lo Mauro, A., Schena, E., Pedotti, A., Sybrecht, G. W., & Aliverti, A. (2010). Breathing pattern and chest wall volumes during exercise in patients with cystic fibrosis, pulmonary fibrosis and COPD before and after lung transplantation. *Thorax*, *65*, 808–814. https://doi.org/10.1136/thx.2009.131409

Worlitzsch, D., Tarran, R., Ulrich, M., Schwab, U., Cekici, A., Meyer, K. C., Birrer, P., Bellon, G., Berger, J., Weiss, T., Botzenhart, K., Yankaskas, J. R., Randell, S., Boucher, R. C., & Döring, G. (2002). Effects of reduced mucus oxygen concentration in airway Pseudomonas infections of cystic fibrosis patients. *Journal of Clinical Investigation*, *109*(3), 317–325. https://doi.org/10.1172/JCI200213870

Yuan, S., Hollinger, M., Lachowicz-scroggins, M. E., Kerr, S. C., Dunican, E. M., Daniel, B. M., & Fahy, J. V. (2015). Oxidation increases mucin polymer cross-links to stiffen airway mucus gels. *Science Translational Medicine*, *7*(276), 276ra27.

Zhang, S., Cui, Z., Wang, Y., & den Toonder, J. M. J. (2020). Metachronal actuation of microscopic magnetic artificial cilia generates strong microfluidic pumping. *Lab on a Chip*, *20*(19), 3569–3581. https://doi.org/10.1039/D0LC00610F

Zhang, S., Wang, Y., Lavrijsen, R., Onck, P. R., & den Toonder, J. M. J. (2018). Versatile microfluidic flow generated by moulded magnetic artificial cilia. *Sensors and Actuators B: Chemical*, *263*, 614–624. https://doi.org/10.1016/j.snb.2018.01.189

Zhang, S., Wang, Y., Onck, P. R., & den Toonder, J. M. J. (2019). Removal of microparticles by ciliated surfaces—an experimental study. *Advanced Functional Materials*, *29*(6), 1806434. https://doi.org/10.1002/adfm.201806434

Zhu, P.-F., Li, X., Li, A., Liu, Y., Chen, D.-D., & Xu, Y.-Q. (2019). Simulation study on the mass transport based on the ciliated dynamic system of the respiratory tract. *Computational and Mathematical Methods in Medicine*, *2019*, 1–9. https://doi.org/10.1155/2019/6036248

SUPPORTING INFORMATION

Additional Supporting Information may be found online in the supporting information tab for this article.

How to cite this article: Pedersoli, L., Zhang, S., Briatico-Vangosa, F., Petrini, P., Cardinaels, R., den Toonder, J., & Peneda Pacheco, D. (2021). Engineered modular microphysiological models of the human airway clearance phenomena. *Biotechnology and Bioengineering*, 118, 3898–3913. https://doi.org/10.1002/bit.27866